Shock Wave Compression of Single-Crystal Forsterite

IAN JACKSON[1] AND THOMAS J. AHRENS

Seismological Laboratory, California Institute of Technology, Pasadena, California 91125

Hugoniot equation of state measurements have been performed on pure synthetic single-crystal forsterite (Mg_2SiO_4) in the pressure range 70–160 GPa (0.7–1.6 Mbar). These and earlier data for polycrystalline forsterite are compared with theoretical Hugoniots for the assemblages 2MgO (rocksalt) + SiO_2 (stishovite) and MgO (rocksalt) + $MgSiO_3$ (perovskite). The densities attained by single-crystal forsterite at pressures in excess of 120 GPa are greater than those expected in the event of shock-induced transformation to the isochemical oxide mixture. A similar test of the hypothesis of shock-induced transformation to the perovskite-bearing assemblage is sensitive to the choice of $MgSiO_3$ (perovskite) bulk modulus. Recent static compression measurements of Yagi et al. (1978) yield a K_{0T} of 286 GPa (for $K_{0T}' = 5$), which, along with other elastic and thermodynamic parameters, suggests that shocked forsterite may be more dense than the perovskite-bearing assemblage. Crystalline phases of up to 5% greater zero-pressure density or equally dense short-range-order-only phases may well be involved. Alternatively, the use of an isentropic bulk modulus of 250 GPa (estimated by Liebermann et al., 1977) for $MgSiO_3$ (perovskite) allows consistency between the data and the calculated MgO + $MgSiO_3$ (perovskite) Hugoniot for a reasonable choice (~ 3.8) of K_{0s}' for the latter phase. The new forsterite data along with high-pressure Hugoniot data for other olivines and olivinitic rocks define a smooth isobaric variation of Hugoniot density with composition. It is shown that an estimated pyrolite (Ringwood, 1975) Hugoniot density of 5.31 g/cm³ at 120 GPa is ~2% less dense than inferred from typical lower mantle density profiles.

INTRODUCTION

For more than a decade, dynamic compression data [e.g., *Trunin et al.*, 1965; *McQueen et al.*, 1967] for rocks rich in forsteritic olivine and enstatitic pyroxene have provided the basis for discussion of the composition and properties of the earth's lower mantle [e.g., *Ahrens et al.*, 1969*a*; *Davies and Gaffney*, 1973; *Jeanloz and Ahrens*, 1977*a*]. All of the available shockwave data for forsterite (synthetic polycrystalline aggregates) and forsteritic (~Fo_{92}) rocks are assembled in Figure 1. The following features are noteworthy.

1. The Twin Sisters dunite (92% Fo_{92}, 9% En_{92}, and 1% chromite by volume [*McQueen et al.*, 1967; *Ahrens and Peterson*, 1969]) and 'Olivinite I' (90% Fo_{90}, 7% biotite, and 3% titanomagnetite by weight [*Trunin et al.*, 1965]) Hugoniot data are quite consistent despite minor differences in rock chemistry and mineralogy. Repeated analysis of these data [*Wang*, 1968; *D. L. Anderson and H. Kanamori*, 1968; *Ahrens et al.*, 1969*a*; *Al'tshuler and Sharipdzhanov*, 1971; *Davies and Anderson*, 1971; *Davies and Gaffney*, 1973] has indicated that the densities attained above 80 GPa (800 kbar) are indistinguishable from those expected for an isochemical mixture of (Mg, Fe)O (rocksalt) and SiO_2 (stishovite). (However, see also *Jeanloz and Ahrens* [1977*a*].)

2. The data of *McQueen and Marsh* [1966] and *Ahrens et al.* [1971] for synthetic forsterite aggregates of 2–5% porosity are also internally consistent but suggest Fo_{100} densities some 2% greater than Fo_{92} densities above 80 GPa. Since it has been generally concluded that the latter are comparable with those of an isochemical oxide mixture, the data for porous Fo_{100} aggregates appear to require the transformation of pure Mg_2SiO_4 to an intrinsically denser phase or assemblage [*Ahrens et al.*, 1969*a*; *Al'tshuler and Sharipdzhanov*, 1971; *Davies and Gaffney*, 1973].

3. Finally, there remain some data [*McQueen*, 1968] for polycrystalline Fo_{100} aggregates of essentially zero porosity (ρ_0 = 3.20 g/cm³) which suggest a smaller (or at least more gradual) increase in density with increasing shock pressure.

In order to resolve the apparent discrepancy between the 'porous' and 'nonporous' forsterite Hugoniots and to futher characterize the relationship between the Fo_{100} and Fo_{92} Hugoniots, we have used a two-stage light-gas gun to study the dynamic compression of pure synthetic single-crystal forsterite (Mg_2SiO_4) in the pressure range 70–160 GPa (700–1600 kbar).

EXPERIMENTAL DETAILS

Rectangular forsterite discs approximately 10 mm × 10 mm in lateral extent and 2.5–3.5 mm in thickness were cut from a large boule grown with the Czochralski technique by the Crystal Products Division of the Union Carbide Corporation. Densities determined by the Archimedean method on 10 such discs during the course of this study averaged 3.222 g/cm³ at 23°C with a standard deviation of 0.002 g/cm³. *Graham and Barsch* [1969] report a density of 3.221$_7$ g/cm³ (25°C) for a crystal of almost ideal composition from the same source, grown by the flame fusion technique [*Shankland*, 1967]. Both zero-pressure bulk densities are slightly greater than the X ray density of 3.214 g/cm³ listed by *Robie et al.* [1966]. After being lapped to within ±0.002 mm of uniform thickness the discs were mounted, along with an array of fused quartz arrival mirrors, on 0.5-mm-thick Al-2024 or Ta driver plates. For all discs the shock propogation direction was within ±3° of (010).

A two-stage light-gas gun [*Jones et al.*, 1966] was used to accelerate plastic projectiles bearing 2.5-mm-thick Al-2024 or Ta flyer plates to velocities in the range 4.0–6.5 km/s. The projectile velocity immediately prior to impact with the stationary driver plate was measured over a ~350-mm path by using two 15-ns duration flash X ray sources (Field Emission Corporation model 539) and 0.01 μs electronic counters to determine the interflash time interval. Uncertainties in path length and time interval between flash X ray exposures result in a final uncertainty of ±0.3% in measured projectile velocities. Instrumental malfunction during some of the early shots in this series necessitated the use of otherwise redundant velocity data of lower precision.

[1] Present address: Research School of Earth Sciences, Australian National University, Canberra, A.C.T. 2600, Australia.

Paper number 8B1114.
0148-0227/79/008B-1114$01.00

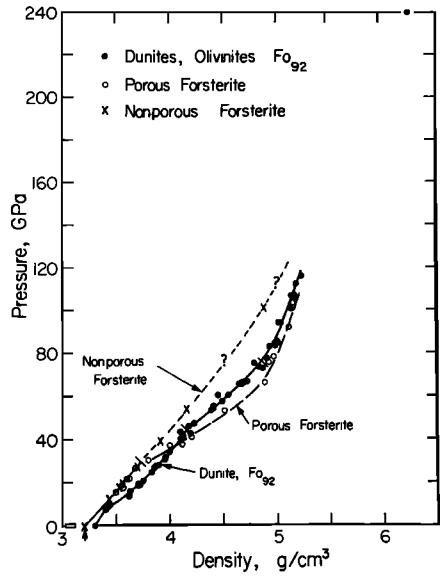

Fig. 1. Hugoniot data for forsterite and forsteritic rocks. The sources of the various data are indicated in the text.

The driver arrival mirrors and sample buffer were illuminated by a 540 J xenon lamp (50-μs duration) and observed through a narrow (0.2 mm) slit by an image converter streak camera writing at 20 mm/μs. Extinction of applied illumination upon shock arrival at each reflecting surface along with shock-induced illumination in the fused quartz mirror material allowed precise measurement of shock transit times through the sample, buffer, and driver arrival mirrors. The streak records so obtained were calibrated by using a modulated laser beam which provided time marks at 50-ns intervals (see *Jeanloz and Ahrens* [1977*a*] for a more complete description of this and other experimental details).

A sensitive microphotometer coupled to a paper chart recorder was used to scan all streak records, allowing accurate determination of illumination onset and extinction times. Such times were defined by the half-intensity points associated with the illumination changes recorded on the paper chart. We assume, on the basis of data obtained from additional mirrors mounted on the fused quartz buffer and arrival mirrors for shot 020, that shock transit times measured from the duration of shock-induced illumination in the fused quartz mirrors are overestimated by 9 ± 2 ns (at least for impact velocities of 5–6 km/s). The shock transit times through the buffer and arrival mirrors in the other experiments were corrected accordingly. Shock transit times through the sample are not dependent on duration of shock-induced illumination and therefore require no such correction. At projectile velocities below 5.8 km/s the variation of arrival mirror applied illumination extinction (or shock-induced illumination onset) time t with lateral distance x across the streak record is linear within the precision of measurement. The variation arises from slight relative inclination (tilt) of the plane surfaces of flyer and driver plates at impact. However, for projectile velocities greater than 5.8 km/s, flyer plate deformation (bowing), well described by quadratic dependence of t on x, complicates the interpretation of streak records. For shots 025 and 020, corrections to the shock transit times (obtained by a quadratic least squares fit to the arrival mirror data) amounted to −8.9 and −3.4 ns, respectively. For shot 021 the arrival mirror data were not of sufficient quality to constrain adequately a quadratic fit; nevertheless, evidence for bowing in the streak record suggested that a substantial correction was required, and consequently, a correction of −9 ns was somewhat arbitrarily applied.

Finally, minor variations (~2%) in streak camera writing rate along the length of the 2-μs streak record have been allowed for by the use of a quadratic fit to the calibration (distance on film versus time) data. Sample shock velocities corrected for projectile bowing and corrected buffer shock velocities are subject to an overall uncertainty of ±1%, while corrected arrival mirror velocities (over shorter paths) are known to within ±2%. Corrections for the minor variations in streak camera writing and the flyer plate deformation account for discrepancies between Table 1 and the results of a preliminary analysis of the same data [*Jackson and Ahrens*, 1977].

DATA REDUCTION

Forsterite Hugoniot States

The measured projectile impact (V_{imp}) and sample shock (U_{ss}) velocities (Table 1) along with the known equations of state [*McQueen et al.*, 1970] of Ta and Al-2024 allow calculation of the particle velocity (u_{ps})-pressure (p_H)-density (ρ_H) state behind the shock wave by the use of the impedance-matching procedure and the Rankine-Hugoniot conservation

TABLE 1. Forsterite Hugoniot and Release Adiabat Data

			Hugoniot State				Partially Released State			
Shot	Flyer, Driver Composition	Impact Velocity (measured) V_{imp}, km/s	Sample Shock Velocity (measured) U_{ss}, km/s	Sample Particle Velocity (calculated) u_{ps}, km/s	Pressure (calculated) P_H, GPa	Density (calculated) ρ_H, g/cm³	Buffer Shock Velocity (measured) U_{sb}, km/s	Sample, Buffer Particle Velocity (calculated) u_{pb}, km/s	Sample, Buffer Pressure (calculated) P_R, GPa	Sample Density (calculated) ρ_R, g/cm³
032	Al-2024	5.15 ± 0.02	8.96 ± 0.09	2.40 ± 0.02	69.2 ± 0.5	4.40 ± 0.03				
030	Ta	4.34 ± 0.02	9.35 ± 0.09	3.16 ± 0.02	95.1 ± 0.9	4.87 ± 0.03	7.03 ± 0.07	3.72 ± 0.04	57.5 ± 1.2	4.68 ± 0.05
028	Ta	4.40 ± 0.02	9.50 ± 0.09	3.19 ± 0.02	97.8 ± 0.9	4.85 ± 0.03	7.20 ± 0.07	3.82 ± 0.04	60.6 ± 1.3	4.61 ± 0.05
023	Ta	5.19 ± 0.05	10.01 ± 0.10	3.77 ± 0.04	121.5 ± 1.6	5.17 ± 0.05	8.60* ± 0.09	4.70 ± 0.06	88.9 ± 2.0	4.54 ± 0.14
025	Ta	5.83 ± 0.02	10.60 ± 0.11	4.22 ± 0.02	144.0 ± 1.3	5.35 ± 0.05	8.93* ± 0.09	4.91 ± 0.06	96.4 ± 2.1	5.08 ± 0.07
020	Ta	6.01 ± 0.06	10.93 ± 0.11	4.33 ± 0.05	152.4 ± 2.0	5.33 ± 0.06	9.42 ± 0.09	5.21 ± 0.06	108.0 ± 2.2	4.87 ± 0.12
021	Ta	6.39 ± 0.13	11.12† ± 0.11	4.61 ± 0.10	165.1 ± 3.9	5.50 ± 0.10				

*Shock transit times determined from the duration of shock-induced illumination have been corrected downwards by 0.009 (±0.003) μs (see text).

†The measured shock transit time through the sample has been reduced by 0.009 μs to allow for deformation of the flyer plate (see text).

TABLE 2. Vitreous Silica Hugoniot Data

Shot	Flyer, Driver Composition	Impact Velocity (measured) V_{imp}, km/s	Shock Velocity (measured) U_s, km/s	Particle Velocity (calculated) u_p, km/s	Pressure (calculated) P, GPa	Density (calculated) ρ, g/cm^3
030	Ta	4.34 ± 0.02	6.62 ± 0.13	3.61 ± 0.02	52.5 ± 0.9	4.83 ± 0.14
028	Ta	4.40 ± 0.02	6.75 ± 0.13	3.65 ± 0.02	54.2 ± 0.9	4.79 ± 0.13
023	Ta	5.19 ± 0.05	7.71* ± 0.15	4.24 ± 0.04	71.9 ± 1.4	4.89 ± 0.15
025A	Ta	5.83 ± 0.02	8.36* ± 0.17	4.73 ± 0.03	87.0 ± 1.5	5.06 ± 0.15
025C	Ta	5.83 ± 0.02	8.68* ± 0.17	4.70 ± 0.02	89.8 ± 1.5	4.80 ± 0.15
020	Ta	6.01 ± 0.06	8.86 ± 0.17	4.84 ± 0.05	94.3 ± 1.8	4.84 ± 0.16

*Shock transit times determined from duration of shock-induced illumination have been reduced by 0.009 (±.003) μs (see text).

equations [see, e.g., *Rice et al.*, 1958]. The relevant expressions for a symmetrical impact (i.e., driver and flyer of the same material) are

Impedance matching

$$u_{ps} = V_{imp} + \{X - (X^2 + 4s^2Y)^{1/2}\}/2s$$
$$X = C_0 + \rho_{0s}U_{ss}/\rho_{0d} \quad (1)$$
$$Y = \rho_{0s}U_{ss}V_{imp}/\rho_{0d}s$$

Conservation of momentum

$$P_H = \rho_{0s}U_{ss}u_{ps} \quad (2)$$

Conservation of mass

$$\rho_H = \rho_{0s}/(1 - u_{ps}/U_{ss}) \quad (3)$$

where ρ_{0s} and ρ_{0d} are the (initial) zero-pressure densities of sample and driver, respectively, and C_0 and s are the coefficients of the linear relation

$$U_s = C_0 + su_p \quad (4)$$

describing the Hugoniot equation of state of the flyer/driver material. Uncertainties in impact velocity ($\sigma[V_{imp}]$) and shock velocity ($\sigma[U_{ss}]$) are assumed to be independent and to propagate [see, e.g., *Jenkins and Watts*, 1968] through to an uncertainty $\sigma(D)$ in any derived parameter D according to the expression

$$\sigma^2(D) = \left(\frac{\partial D}{\partial V_{imp}}\right)^2\sigma^2(V_{imp}) + \left(\frac{\partial D}{\partial U_{ss}}\right)^2\sigma^2(U_{ss}) \quad (5)$$

The partial derivatives required in the calculation of $\sigma(u_{ps})$, $\sigma(P_H)$, and $\sigma(\rho_H)$ are presented in the appendix. The measured and calculated parameters and their associated uncertainties are presented in Table 1.

Fused Quartz Hugoniot States

The Hugoniot states attained in the fused quartz arrival mirrors were determined similarly and are presented in Table 2 and Figure 2. These six states, along with the data of *Wackerle* [1962] and *Jones et al.* [1968] for $U_p > 2.5$ km/s, are well described ($r^2 = 0.9912$) by a linear $U_s - u_p$ relation (equation (4)) with $C_0 = 1.0861$ km/s and $s = 1.5990$. This Hugoniot equation of state for fused quartz will be used in the following section to extract forsterite release adiabat information from the measured buffer shock velocities.

Forsterite Partially Released States

Interaction of the primary shock wave propagating within the sample with an interface between the sample and a buffer of lower shock impedance results in transmission of a shock wave (of lesser amplitude) into the buffer and reflection of a partial rarefaction into the samples [see, e.g., *Ahrens et al.*, 1969*b*]). Boundary conditions at the interface require that these transmitted and reflected waves produce a common (P, u_p) state in the sample and buffer. Measurement of buffer shock velocity U_{sb} in a buffer of known equation of state ($U_{sb} = C_{0b} + s_bu_{pb}$) thus allows determination of the (P, u_p) state in the partially released sample by application of (2). The (P_R, u_{pb}) states so determined are presented in Table 1. If the partial rarefaction is isentropic, the change in the flow is described by the Riemann integral [e.g., *Rice et al.*, 1958]:

$$u_{pb} - u_{ps} = -\int_{P_H}^{P_R}\left(-\frac{\partial V}{\partial P}\right)_s^{1/2} dP \quad (6)$$

It has been demonstrated [*Lyzenga and Ahrens*, 1978] that integration of (6) over a linear P-V path yields an upper bound

$$\rho_R = \{1/\rho_H + (u_{pb} - u_{ps})^2/(P_H - P_R)\}^{-1} \quad (7)$$

for the density of the partially released (P_R, u_{pb}) state. Densities calculated from (7) are presented in Table 1. Error propagation has been treated as it was for the Hugoniot state with the necessary partial derivatives included in the appendix.

EXPERIMENTAL RESULTS

The new Hugoniot data for single-crystal forsterite and the polycrystalline forsterite data of Figure 1 are plotted in (u_p, U_s) space in Figure 3. For particle velocities in the range 1.0–3.5 km/s the new data and those of *McQueen* [1968] for

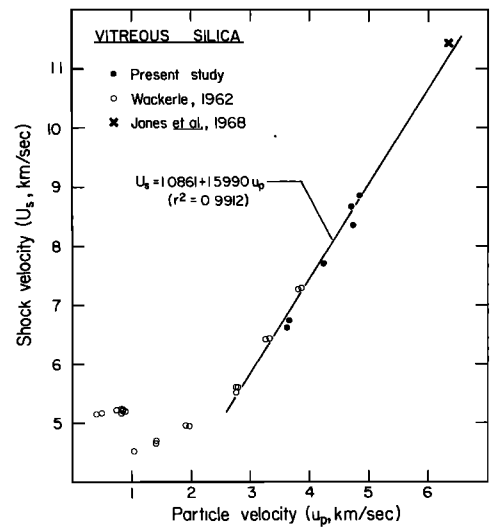

Fig. 2. Vitreous silica Hugoniot data in the (u_p, U_s) plane.

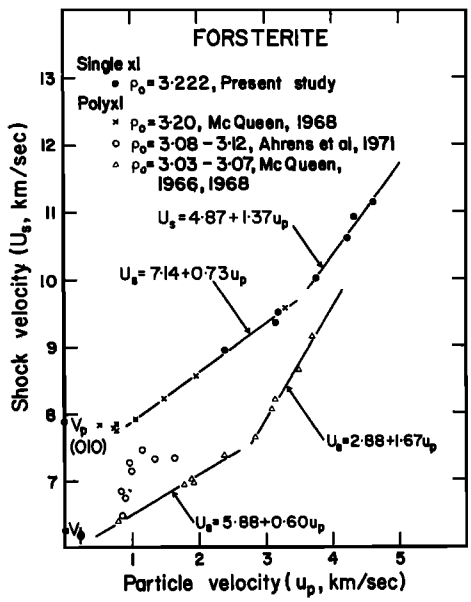

Fig. 3. Forsterite Hugoniot data in the (u_p, U_s) plane. The appropriate longitudinal (V_p, 010) and bulk sound (V_ϕ) velocities are from *Graham and Barsch* [1969].

nonporous aggregates form an internally consistent set well described (r^2 = 0.99) by the linear least squares fit:

$$U_s = 7.14 + 0.73u_p \quad (8)$$

For particle velocities greater than 3.5 km/s a second linear $U_s - u_p$ trend is evident:

$$U_s = 4.87 + 1.37u_p \qquad r^2 = 0.97 \quad (9)$$

The steep slope of the latter and the location of the corresponding (ρ, P) trajectory (Figure 5) suggest that (9) describes the homogeneous compression of Mg_2SiO_4 in a less compressible shock-induced high-density state. Equation (8) describes the anomalously compressible behavior of Mg_2SiO_4 as it progressively transforms (with increasing shock pressure) to this high-pressure phase or state.

Furthermore, it is evident from Figure 3 that the data of *McQueen and Marsh* [1966] reveal a qualitatively identical (u_p, U_s) trend with two well-defined linear segments. The following three important questions arise from this analysis of the data of Figure 3.

1. Do the linear $u_p - U_s$ segments evident at large particle velocities in both the nonporous and porous data sets correspond to the homogeneous compression of the same high-pressure phase or state?
2. If so, what is the nature of this dense and incompressible material?
3. Why is this high-pressure state so much more readily achieved by shock compression of porous rather than nonporous forsterite?

Before exploring these questions in detail, it is appropriate to consider the data for partially released states and the information they provide concerning the nature of dynamically compressed states.

Forsterite Partially Released States

Pressure-density states attained in the forsterite samples behind partial rarefaction waves propagating from the sample-buffer interface (see Table 1) have been plotted along with all forsterite Hugoniot data in Figure 4. With the exception of one unexplained anomaly (shot 023) the release paths (connecting Hugoniot and associated partially released states) are strikingly parallel to that part of the single-crystal Hugoniot which represents homogeneous compression of the shock-induced high-pressure state. The general steepness of these release adiabats is consistent with other recent studies [*Ahrens et al.*, 1969*b*; *Grady et al.*, 1974] which revealed release paths much steeper (greater $\partial P/\partial \rho$) than corresponding Hugoniots for plagioclase and quartz shocked to states within the regions of anomalously large compressibility on their respective Hugoniots. (These regions are often referred to as 'mixed phase regimes' beyond which it is traditionally assumed that shock-induced transformation to high-pressure phases or states is complete.) Collectively, these studies suggest that shock-induced high-pressure states in shocked silicates survive at least the initial stages of the unloading process. The fact that recent shock recovery experiments on natural single-crystal olivine [*Jeanloz and Ahrens*, 1977*b*; *Jeanloz et al.*, 1977] shocked well into the Twin Sisters dunite 'mixed phase regime' reveal little evidence of extensive shock-induced phase transformation seems therefore to require retrogressive transformation during the later stages of pressure release.

Discussion

In order to assess the forsterite Hugoniot data more quantitatively, theoretical Hugoniots for various Mg_2SiO_4 phases have been constructed after the manner of *McQueen et al.* [1963] (see also *Davies and Gaffney* [1973]). The Hugoniot pressure P_H at a given density ρ is related to the appropriate principal isentrope $P_s(\rho)$ through the Mie-Grüneisen description of the thermal equation of state:

$$P_H = \{P_S - \gamma\rho(\Delta U_s + E_{TR})\}/\{1 - \gamma(\rho/\rho_0' - 1)/2\} \quad (10)$$

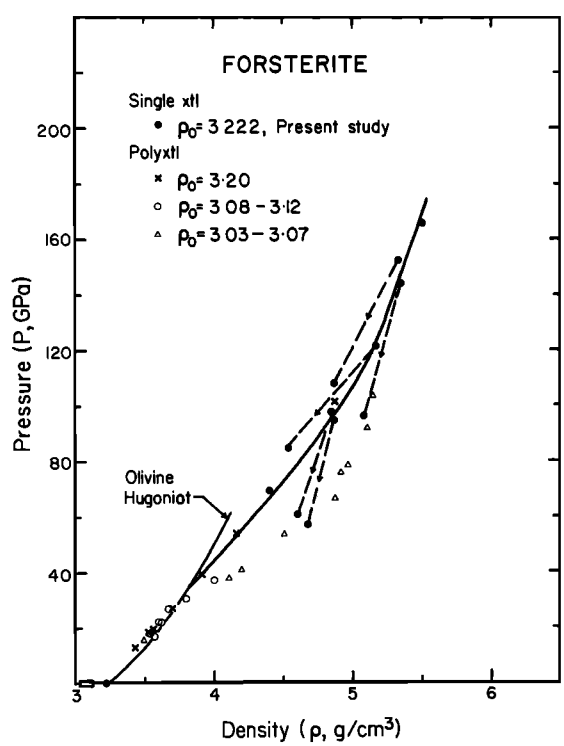

Fig. 4. Forsterite Hugoniot and release adiabat states. The heavy solid line is the nonporous forsterite Hugoniot, while the dashed lines connect Hugoniot and partially released states observed in the present study. The curve 'Olivine-Hugoniot' is the theoretical Hugoniot for the olivine structure transposed from Figure 5.

TABLE 3. Parameters Used in Calculation of Theoretical Hugoniots

Parameter	Mg_2SiO_4 (olivine)	2MgO (rocksalt) + SiO_2 (stishovite)	MgO (rocksalt) + $MgSiO_3$ (perovskite)
ρ_0, g/cm³	3.222	3.85	3.93*
K_{0s}, GPa	129†	201 ± 15‡	219 ± 20‡ 239 ± 20‡
K_{0s}'	5.2†	4.7 ± 0.6§	4.7 ± 1.2§
γ_0 ||	1.15	1.5 ± 0.5	1.5 ± 0.5
n ||	1.0	1.5 ± 0.5	1.5 ± 0.5
E_{TR}, || KJ/g	0	1.0 ± 0.5	1.0 ± 0.5
ρ_0', g/cm³	3.222	3.222	3.222

*Using ρ_0 = 4.09 g/cm³ for $MgSiO_3$ (perovskite). This is close to the mean of the densities reported by *Liu* [1975], E. Ito (personal communication, 1977), and *Yagi et al.* [1977].

†VRH average of single-crystal moduli [*Graham and Barsch*, 1969; *Kumazawa and Anderson*, 1969].

‡Voigt-Reuss-Hill (VRH, see *Hill* [1952]) averages of the following moduli: MgO, 163 GPa [*Spetzler*, 1970]; SiO_2 (stishovite), 280 ± 30 GPa [*Liebermann et al.*, 1976]; $MgSiO_3$ (perovskite), 250 ± 30 GPa [*Liebermann et al.*, 1977], 286 ± 30 GPa [*Yagi et al.*, 1978].

§Voigt-Reuss-Hill values based on K_{0s}' (MgO) = 3.9 [*Spetzler*,] 1970] and estimates of 6 ± 2 and 5 ± 2, for K_{0s}' of stishovite and $MgSiO_3$ (perovskite), respectively, from data for structural analogues.

|| In the absence of any data suggesting otherwise, γ_0, n, and E_{TR} are assumed to be the same for both high-pressure assemblages. The γ_0 and n values are typical of those for close packed oxides [see, e.g., *Davies*, 1974], whereas E_{TR} has been estimated after the manner of *Jeanloz and Ahrens* [1977*a*]. The γ_0 for forsterite was calculated from available thermodynamic data [*O. L. Anderson et al.*, 1968].

In the above, ρ_0', γ, and E_{TR} are the initial density of the shocked material, the Grüneisen parameter, and the energy change at zero pressure associated with any shock-induced phase transformation, respectively. The density dependence of the Grüneisen parameter was assumed to be of the form:

$$\gamma = \gamma_0(\rho_0/\rho)^n \tag{11}$$

ΔU_s is the internal energy change along the principal isentrope between the zero-pressure density ρ_0 and the given density:

$$\Delta U_s = \int_{\rho_0}^{\rho} P_s \, d\rho/\rho^2 \tag{12}$$

Third-order Eulerian (Birch-Murnaghan) principal isentropes,

$$P_s(\rho) = \frac{3K_{0s}}{2}\{(\rho/\rho_0)^{7/3} - (\rho/\rho_0)^{5/3}\} \cdot\{1 + \tfrac{3}{4}[K_{0s}' - 4][(\rho/\rho_0)^{2/3} - 1]\}\} \tag{13}$$

were based, where possible, on ultrasonically determined bulk moduli (K_{0s}) and first pressure derivatives (K_{0s}') and elsewhere on K_0 and K_0' values measured by static compression or inferred from data for isostructural analogues.

Theoretical Hugoniots, centered on olivine (ρ_0' = 3.222 g/cm³), have been calculated for untransformed olivine and for the possible high-pressure assemblages 2MgO (rocksalt) + SiO_2 (stishovite) and MgO (rocksalt) + $MgSiO_3$ (orthoperovskite) by using the parameters of Table 3. Envelopes of uncertainty associated with the mixed oxide and perovskite-bearing assemblages (e.g., Figure 5) were obtained by independently varying each of the model parameters within the stated uncertainties (Table 3). Comparison of the Hugoniot data with the calculated Hugoniots reveals the following important features.

1. At pressures below 35 GPa all data are consistent with the survival of the olivine crystal structure under conditions of shock compression (see Figure 5).

2. The highest-pressure data (P > 120 GPa) of the present study are characterized by densities too large to be consistent with the hypothesis of shock-induced transformation of forsterite to its isochemical oxide mixture 2 MgO (rocksalt) + SiO_2 (stishovite).

3. Interpretation of the same data in terms of the calculated Hugoniots for the perovskite-bearing assemblage is complicated by the considerable uncertainty in both K_{0s} and K_{0s}' for $MgSiO_3$ (perovskite).

On the one hand, K_{0s} for $MgSiO_3$ (perovskite) has been estimated as 250 ± 30 GPa [*Liebermann et al.*, 1977] on the basis of fairly well established bulk sound velocity (v_ϕ)—mean atomic weight ($\bar{m}$) systematics for isostructural analogues. Use of this value yields a (VRH) K_{0s} of 219 ± 20 for the assemblage. Calculation of the associated envelope of uncertainty (half-hatched in Figure 5) by independent variation of the various parameters within the stated uncertainties (Table 3) shows that the densities attained by shocked forsterite at pressures greater than 120 GPa are consistent with the hypothesis of shock-induced transformation of olivine to the assemblage MgO (rocksalt) + $MgSiO_3$ (perovskite)—the post spinel assemblage observed by *Liu* [1975, 1976] in static high-pressure studies. Variation of the various parameters of Table 3 within the stated uncertainties demonstrates that the calculated Hugoniot is most sensitive to variation of K_{0s}'. It thus seems appropriate to vary K_{0s}' (fixing all other parameters at their preferred values) to obtain the theoretical Hugoniot which best fits the four highest-pressure Hugoniot data. The resulting K_{0s}' for the assemblage of MgO + $MgSiO_3$ (perovskite) of 3.8 lies well within the allowed range (see Table 3 and Figure 5) and implies that K_{0s}' for $MgSiO_3$ (perovskite) itself is also 3.8.

On the other hand, recent static compression measurements by *Yagi et al.* [1978] suggest an $MgSiO_3$ (perovskite) bulk modulus of 286 GPa for an assumed K' of 5. Consideration of the bulk modulus of the isochemical mixture MgO (K_{0s} = 163 GPa) + SiO_2 (stishovite, K_{0s} = 280 ± 30 GPa), which is only 2% less dense, along with the above mentioned systematics, suggests that the measured modulus is surprisingly high. For this reason and because of the considerable difficulty of accurate bulk modulus determination by static compression for crystals of such low symmetry (orthorhombic), both the measured and the estimated K_0 are used in the present analysis. Use of the Yagi et al. K_0 (the difference between K_{0T} and K_{0s} can be neglected) along with the other parameters of Table 3 yields the hatched envelope of uncertainty in Figure 5. The higher K_{0s} clearly renders consistency between the data and the calculated Hugoniots for the perovskite phase somewhat more marginal. For consistency a K_{0s}' value of ~3.5 is required for the assemblage (all other parameters remaining fixed at their preferred values). The implied $MgSiO_3$ (perovskite) K_{0s}', which depends on the assumptions made in calculating the elastic properties of the two-phase aggregate, lies in the range 2.2 (Reuss) 3.3 (Voigt).

4. The highest-pressure data for porous polycrystalline forsterite aggregates [*McQueen and Marsh*, 1966] display densities too large to be consistent with shock-induced transformation of olivine to either the mixed-oxide (see also *Ahrens et al.* [1969*a*] and *Davies and Gaffney* [1973]) or the perovskite-bearing assemblage. In the latter case a density discrepancy of about 3% is evident (see Figure 5). Another measure of this discrepancy is obtained by requiring that the high-pressure

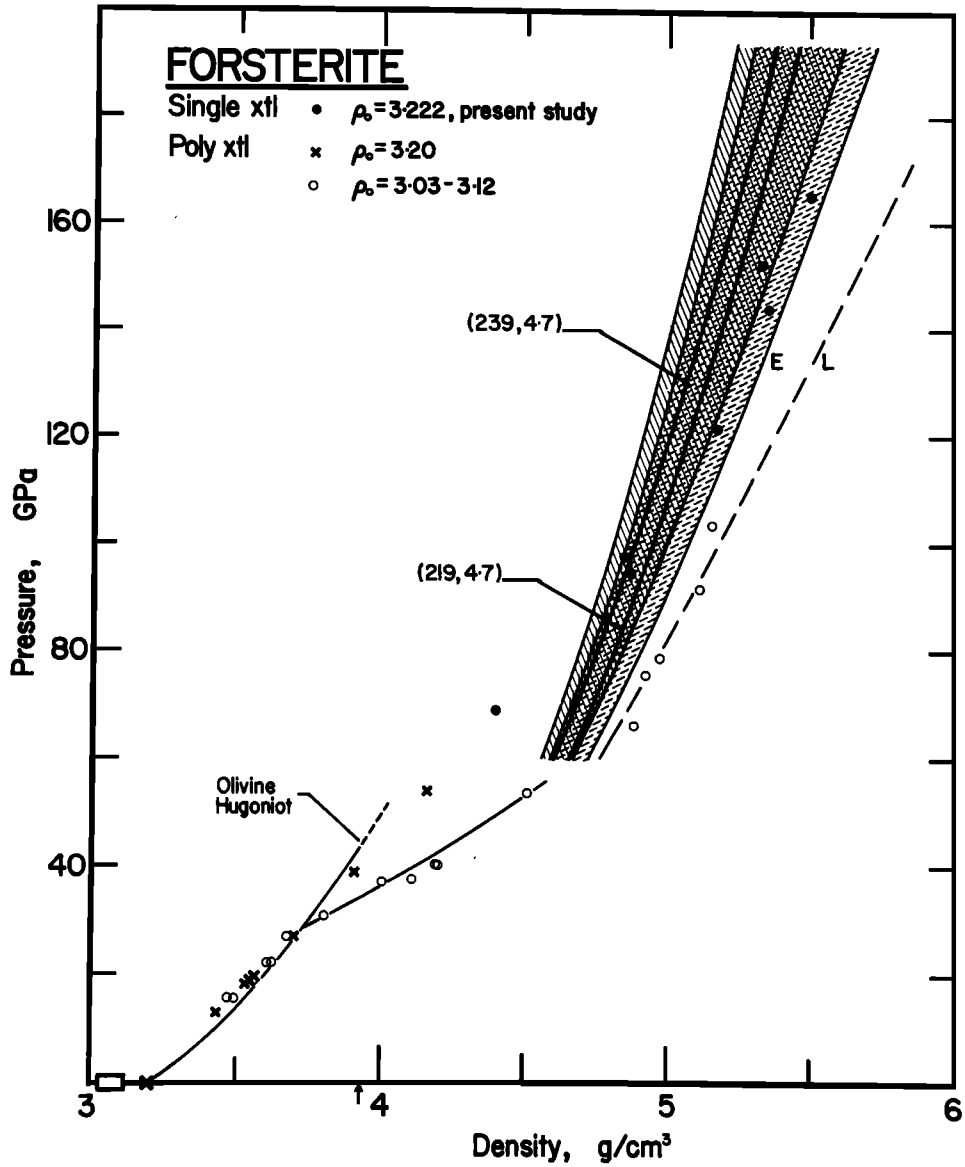

Fig. 5. A comparison of forsterite Hugoniot data with calculated Hugoniots for untransformed olivine and for the high-pressure assemblage MgO (rocksalt) + $MgSiO_3$ (perovskite). The heavy curve labeled (219, 4.7) corresponds to the choice of a third-order Eulerian isentrope with K_{0s} = 219 GPa, K_{0s}' = 4.7, and all other parameters fixed at their preferred values (Table 3). Independent variation of each parameter within the stated uncertainties yields the associated envelope of uncertainty (half-hatched). The high- (curve *E*) and low-density margins of the envelope correspond to K_{0s}' values of 3.5 and 5.9, respectively (see text). The heavy curve labeled (239, 4.7) and the associated envelope of uncertainty (hatched) have the same significance with respect to the alternative choice of K_{0s} (239 GPa). The dashed line *L* is characterized by the same parameters as curve *E* but is based on a third-order Lagrangian isentrope.

data for both the single-crystal and the porous polycrystalline samples be well fitted by a single theoretical Hugoniot based on a third-order Eulerian isentrope with fixed ρ_0(equal to 3.93 g/cm³), γ_0, n, E_{TR} (Table 3) but variable K_{0s} and K_{0s}'. A least squares analysis of this kind yields K_{0s} = 103 GPa and K_{0s}' = 9.6, which are clearly unreasonable values for a close-packed high-pressure phase.

This discrepancy in density between the 'high-pressure phases' of the initially porous and initially nonporous samples is not the only difficulty to be overcome in reconciling these two sets of data. It is also evident (Figure 5) that the porous samples display a much greater compressibility than their nonporous counterparts in the pressure range 30–70 GPa. *Jeanloz and Ahrens* [1977*a*] (see also *McQueen et al.* [1967, 1970]) have suggested that the anomalous relationship between the Hugoniots for porous and nonporous olivines (and pyroxenes) is due to more favorable transformation kinetics associated with larger internal energies in the former. This explanation for the greater ease of phase transformation in initially porous Mg_2SiO_4 in terms of a thermally activated reaction mechanism (see also *Grady* [1977]) may not be the only possibility. For example, there is a suggestion [*de Carli and Jamieson*, 1961] that the wide discrepancy between the Hugoniots of pyrolitic graphite on the one hand and natural and porous 'commercial' graphite on the other is a consequence of microstructural differences. In particular, the absence of stacking faults (which occur in natural graphite) in pyrolitic graphite delays the onset of anomalous compression (traditionally associated with the graphite → diamond transition) to pressures in excess of 40 GPa (400 kbar). Natural graphite and porous commercial graphite, on the other hand, share a common Hugoniot which crosses a calculated graphite Hugoniot (in the direction of

higher densities) at pressures (~5 GPa) approaching the equilibrium graphite ⇄ diamond transition pressure. Conceivably, similar differences in initial defect concentrations between the single-crystal and the nonporous polycrystalline forsterite, on the one hand, and porous polycrystalline samples on the other might contribute to the discrepancies between the respective Hugoniots.

The relative roles of porosity, polycrystallinity, and intracrystalline defects in the process of dynamic yielding and densification clearly remain to be resolved. As a consequence, no unambiguous explanation of the discrepancy between Hugoniot data for porous and nonporous forsterite is yet available. Until it is, we believe that the data from the present study of pure, well-characterized, single-crystal forsterite represents the more reliable guide to the ultra-high-pressure behavior of Mg_2SiO_4.

Finally, one important qualification should be made concerning the derivations of K_{0s}' for $MgSiO_3$ (perovskite) from the Hugoniot data presented above. The comparison of data and calculated Hugoniots is being performed at pressures approaching the zero-pressure bulk moduli of the candidate high-pressure phases. For this reason, such comparisons may be sensitive to the assumptions made in constructing isentropes from the low-pressure ultrasonic data. In particular, the conclusions reached may depend on choice of strain measure (Eulerian versus Lagrangian) and the term at which the energy-strain series is truncated. The importance of the latter is difficult to assess, since no data exist which would facilitate choice of K_0'' which must be explicitly specified in any fourth-order (or higher-order) equation of state. The sensitivity of the comparison to choice of strain measure has, however, been assessed by calculation of theoretical Hugoniots for the MgO + $MgSiO_3$ (perovskite) assemblage based on third-order Lagrangian isentropes of the form [e.g., *Davies*, 1973]

$$P_s(\rho) = \frac{3K_{0s}}{2}\left(\frac{\rho}{\rho_0}\right)^{1/2}\left[1-\left(\frac{\rho}{\rho_0}\right)^{-2/3}\right] \cdot \left\{1+\frac{3K_{0s}'}{4}\left[1-\left(\frac{\rho}{\rho_0}\right)^{-2/3}\right]\right\} \quad (14)$$

One such Hugoniot with K_{0s} = 219 GPa, K_{0s}' = 3.5, and the preferred values (Table 3) of γ_0, n, and E_{TR} is compared with the data and the corresponding Hugoniots based on third-order Eulerian isentropes in Figure 5. For a given K_{0s}' the Lagrangian description (curve L) yields much greater compressibility at high pressure than its Eulerian counterpart (curve E). As a consequence, a much larger K_{0s}' (~5.9) is required if the data are to be described by the Hugoniot based on the Lagrangian isentrope. The corresponding K_{0s}' for $MgSiO_3$ (perovskite) itself is 7.0. It is thus clear that the conclusions are quite sensitive to the choice of equation of state. However, *Davies'* [1973] comparison of calculated Hugoniots for MgO based on third-order Eulerian and Lagrangian isotherms suggests that the former description is to be strongly preferred.

In conclusion, interpretation of our new data for shocked single-crystal forsterite is quite sensitive to the choice of K_{0s} for $MgSiO_3$ (perovskite). Use of the *Liebermann et al.* [1977] estimate (250 ± 30 GPa) suggests compatibility between the data (P > 120 GPa) and the calculated Hugoniot for the perovskite-bearing assemblage for a K_{0s}' of ~3.8 for the perovskite phase. If, on the other hand, the measured K_0 (286 GPa, *Yagi et al.* [1978]) is used, compatibility requires a rather low K_{0s}' (2.2–3.3).

While the above suggests the possibility of consistency (for appropriate K_{0s}, K_{0s}', etc.) between the shock-induced high-pressure state and the MgO (rocksalt) + $MgSiO_3$ (perovskite) assemblage, the identity of the former is by no means established. We have already seen that analysis using the K_0 of *Yagi et al.* [1978] suggests the possibility of modest increases in zero-pressure density beyond 3.93 g/cm³. Such densities might be associated with very close packed short-range-order-only phases (there being no guarantee of long range order in shocked silicates) or with the transformation of Mg_2SiO_4 to denser perovskite-related structures [e.g., *Jeanloz and Ahrens*, 1977*a*; *Liu*, 1978*a*] or the calcium ferrite structure [*Liu*, 1977] and may be consistent with the Hugoniot data provided that K_{0s} and K_{0s}' adopt appropriate values. Specifically, a 5% increase in ρ_0 (from 3.93 to 4.13 g/cm³) accompanied by a 15% increase in K_{0s} (from 219 to 252 GPa g/cm³) is consistent with the data for K_{0s}' ~ 4.7. Larger increases in zero-pressure density would, however, be difficult to reconcile with the Hugoniot data.

IMPLICATIONS FOR THE CONSTITUTION OF THE EARTH'S LOWER MANTLE

As was suggested in the introduction, seismically derived lower mantle pressure-density-incompressibility profiles have traditionally been interpreted on the basis of shock wave data for olivinitic and pyroxenitic rocks. For example, the composition (mole fraction Mg/(Mg + Fe)) of an assumed olivine mantle might be inferred from a comparison of P-ρ profiles from recent earth models with Hugoniot data for olivines of various compositions (see Figure 6). The inversion of the usual density dependence on composition, evident in a comparison of the porous Fo_{100} [*McQueen and Marsh*, 1966] and Fo_{92} [*Trunin et al.*, 1965; *McQueen et al.*, 1967] data, has seriously complicated interpolation among the various olivine Hugoniots to obtain the composition of an olivine mantle. However, the new data for single-crystal forsterite clearly display lower densities at a given pressure than the ~Fo_{92} rocks, in accord

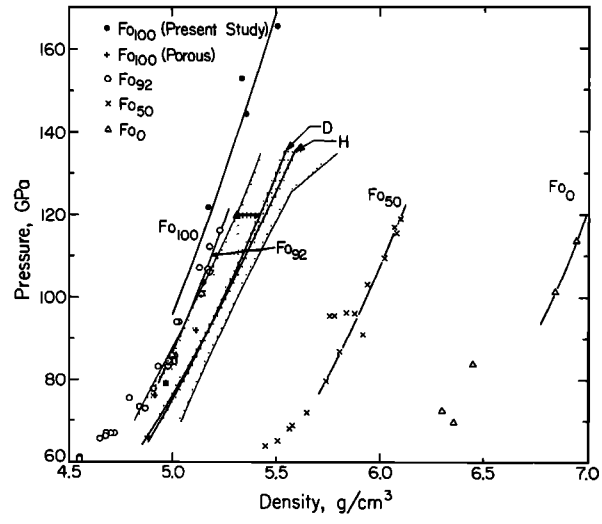

Fig. 6. A comparison of Hugoniot data for olivines of various compositions with (P, ρ) profiles for the earth's lower mantle. Curves D and H are the models of *Dziewonski et al.* [1975] and *Hart* [1977], respectively, while the stippled area represents the range of acceptable density profiles defined by *Worthington* [1973]. The large triangle denotes the calculated pyrolite density at 120 GPa, while the arrow indicates the variation expected for a 1–2 × 10³ decrease in temperature. The Fo_{50} and Fo_0 data are from *McQueen et al.* [1967] and *McQueen and Marsh* [1966], respectively.

TABLE 4. Compositions of Pyrolite and a Chemically Equivalent Combination of Key Rocks and Minerals

	Composition, wt %
*Pyrolite**	
$(Mg_{0.916}Fe_{0.080}Ni_{0.004})_2SiO_4$	52.8
$(Mg_{0.857}Fe_{0.139}Mn_{0.004})SiO_3$	35.4
$CaSiO_3$	6.4
Al_2O_3	4.6
Cr_2O_3	0.3
Fe_2O_3	0.3
TiO_2	0.2
Total	100.0
DBWC†	
$(Mg_{0.915}Fe_{0.081}Ni_{0.003}Mn_{0.001})_2SiO_4$†	52.9
$(Mg_{0.852}Fe_{0.145}Mn_{0.003})SiO_3$†	35.3
$CaSiO_3$	6.4
Al_2O_3	4.6
Cr_2O_3	0.6
Fe_2O_3	0.2
Total	100.0

*Recalculated after removal of trace Na_2O, K_2O, and P_2O_5.

†Twin Sisters dunite composition based on 92 vol % Fo_{92} + 7% En_{92} + 1% chromite (see *Birch* [1960] and *Ragan* [1967] for general petrography and *Ross et al.* [1954] and *Birch* [1961] for mineral analyses). Stillwater bronzitite whole rock analysis [*Hess and Phillips*, 1940; *Birch*, 1961]. The mass fractions of olivine and pyroxene have been adjusted slightly to allow for the slightly different compositions (and thus densities) of the dunite and bronzitite olivines and pyroxenes.

with their different initial densities. Moreover, the new data for Fo_{100} along with the existing data for the Twin Sisters dunite (Fo_{92}), Mooihoek dunite (Fo_{50}), and fayalite (Fo_0) define an impressive linear correlation between 120-GPa Hugoniot density and composition:

$$\rho = 7.00 - 0.018\{MgO/(MgO + FeO)\} \quad (15)$$

yielding an olivine model mantle composition of about Fo_{85}.

Alternatively, one may assess the plausibility of a proposed mantle composition by adding the Hugoniot densities (at a given pressure) for either its oxide components [*Al'tshuler and Sharipdzhanov*, 1971] or its mineral phases [*Ahrens et al.*, 1977]. In particular, *Ringwood*'s [1975] pyrolite may be conveniently expressed to a very good approximation as a linear combination of rocks and minerals whose Hugoniots are either known or readily estimated. The appropriate linear combination (DBWC) in weight percent is: 56.9, Twin Sisters dunite; 34.4, Stillwater bronzitite; 4.8, wollastonite ($CaSiO_3$); and 3.9, corundum (Al_2O_3) which is compared with pyrolite in Table 4. Hugoniot densities of the Twin Sisters dunite, Stillwater bronzitite, and corundum at 120 GPa (1.2 Mbar) are 5.26, 5.40 [*McQueen et al.*, 1967], and 5.16 g/cm³, respectively [*McQueen and Marsh*, 1966], whereas the density of $CaSiO_3$ is estimated to be 5.3 g/cm³ (R. Jeanloz, personal communication, 1977). Addition of these component Hugoniot densities [e.g., *Ahrens et al.*, 1977] yields an estimated pyrolite Hugoniot density (at 120 GPa) of 5.31 g/cm³.

Comparison of this estimated pyrolite density with density profiles obtained by inversion of free oscillation data requires an understanding of the uncertainties inherent in the quantities being compared. For example, a great deal of effort has been expended in recent years on inversion of increasingly large free oscillation data sets for the earth's density distribution, inversion based on the strategy of refinement modeling. The resulting models are generally in close agreement (see, e.g., the *Dziewonski et al.* [1975] and *Hart* [1977] models in Figure 6). *Cleary and Anderssen* [1979] argue, however, that the variability among such models does not necessarily provide a reliable estimate of the inherent nonuniqueness and that the latter should be assessed by application of alternative inversion strategies. By employing linear programing techniques, *Worthington* [1973] obtained bounds (see Figure 6) which reflect the degree of nonuniqueness involved in estimation of lower mantle densities. Thus the estimated pyrolite density of Figure 6 is about 2% less than the (refinement) model densities at the same pressure.

Possible errors may also be introduced into such a comparison by differences in phase and temperature between the mantle and selected Hugoniots [see, e.g., *Wang*, 1968; *Davies*, 1974]. For example, the process by which the Hugoniot density of pyrolite is expressed in terms of known or estimated Hugoniots of appropriate (essentially monominerallic) rocks and minerals excludes the possibility of combination of these minerals in even denser phases. However, reaction among any free (Mg, Fe)O (resulting, for example, from spinel disproportionation) and the $CaSiO_3$ and Al_2O_3 components of pyrolite may result in the formation of ultradense phases like the ϵ-$MgAl_2O_4$ and sodium titanate type $Ca_2Al_2SiO_7$ recently reported by *Liu* [1978*a*, *b*]. Calculations suggest that the presence of such phases would raise the estimated pyrolite density at 120 GPa by no more than 0.04 g/cm³. Alternatively, a temperature difference of $1\text{–}2 \times 10^3$ between mantle and shocked pyrolite at the same pressure would result in a density discrepancy of the order of 0.1 g/cm³. Since estimated shock temperatures for the Twin Sisters dunite and Stillwater bronzitite are of the order of 3000 (±1000?) K at 120 GPa [*Ahrens et al.*, 1969*a*], resolution of the 2% density contrast between pyrolite and the refinement models by temperature differences alone would appear to require quite modest, but not implausibly small, temperature gradients in the earth's lower mantle.

APPENDIX

The partial derivatives required in the calculations of uncertainties in u_{ps}, P_H, and ρ_H from (5) and obtained from (1)–(3) are

$$\frac{\partial u_{ps}}{\partial V_{imp}} = 1 - \frac{\rho_{0s}U_{ss}}{2s\rho_{0d}}(X^2 + Y)^{-1/2} \quad (A1)$$

$$\frac{\partial u_{ps}}{\partial U_{ss}} = \frac{\rho_{0s}}{2s\rho_{0d}}\{1 - (X + V_{imp})(X^2 + Y)^{-1/2}\} \quad (A2)$$

$$\frac{\partial P_H}{\partial V_{imp}} = \rho_{0s}U_{ss}\frac{\partial u_{ps}}{\partial V_{imp}} \quad (A3)$$

$$\frac{\partial P_H}{\partial U_{ss}} = \rho_{0s}u_{ps} + \rho_{0s}U_{ss}\frac{\partial u_{ps}}{\partial U_{ss}} \quad (A4)$$

$$\frac{\partial \rho_H}{\partial V_{imp}} = \frac{\rho_{0s}}{U_{ss}}\frac{\partial u_{ps}}{\partial V_{imp}}\Big/\left(1 - \frac{u_{ps}}{U_{ss}}\right)^2 \quad (A5)$$

$$\frac{\partial \rho_H}{\partial U_{ss}} = \frac{\rho_{0s}}{U_{ss}}\left(\frac{\partial u_{ps}}{\partial U_{ss}} - \frac{u_{ps}}{U_{ss}}\right)\Big/\left(1 - \frac{u_{ps}}{U_{ss}}\right)^2 \quad (A6)$$

Since the partially released state is defined by

$$u_{pb} = (U_{sb} - C_{0b})/s_b \quad (A7)$$

$$P_R = \rho_{0b}U_{sb}u_{pb} \quad (A8)$$

$$\rho_R = \{1/\rho_H + (u_{pb} - u_{ps})^2/(P_H - P_R)\}^{-1} \quad (6)$$

and the errors in U_{ss}, u_{sb}, and V_{imp} are independent, the error propagation is given by expressions of the form

$$\sigma^2(D) = \left(\frac{\partial D}{\partial V_{imp}}\right)^2 \sigma^2(V_{imp}) + \left(\frac{\partial D}{\partial U_{ss}}\right)^2 \sigma^2(U_{ss}) + \left(\frac{\partial D}{\partial U_{sb}}\right)^2 \sigma^2(U_{sb}) \quad \text{(A9)}$$

with the following partials:

$$\frac{\partial u_{pb}}{\partial V_{imp}} = \frac{\partial u_{pb}}{\partial U_{ss}} = 0 \qquad \frac{\partial u_{pb}}{\partial U_{sb}} = 1/s_b \quad \text{(A10)}$$

$$\frac{\partial P_R}{\partial V_{imp}} = \frac{\partial P_R}{\partial U_{ss}} = 0 \qquad \frac{\partial P_R}{\partial U_{sb}} = \frac{\rho_{0b}}{s_b}(2U_{sb} - C_{0b}) \quad \text{(A11)}$$

$$\frac{\partial \rho_R}{\partial V_{imp}} = \rho_R{}^2\left\{\left(\frac{\partial \rho_H}{\partial V_{imp}}\right)\Big/ \rho_H{}^2 + 2\left(\frac{\partial u_{ps}}{\partial V_{imp}}\right)\frac{u_{pb} - u_{ps}}{P_H - P_R} + \left(\frac{\partial P_H}{\partial V_{imp}}\right)\frac{(u_{pb} - u_{ps})^2}{(P_H - P_R)^2}\right\}$$

$$\frac{\partial \rho_R}{\partial U_{ss}} = \rho_R{}^2\left\{\left(\frac{\partial \rho_H}{\partial U_{ss}}\right)\Big/ \rho_H{}^2 + 2\left(\frac{\partial u_{ps}}{\partial U_{ss}}\right)\frac{u_{pb} - u_{ps}}{P_H - P_R} + \left(\frac{\partial P_H}{\partial U_{ss}}\right)\frac{(u_{pb} - u_{ps})^2}{(P_H - P_R)^2}\right\}$$

$$\frac{\partial \rho_R}{\partial U_{sb}} = -\rho_R{}^2 2\left(\frac{\partial u_{pb}}{\partial U_{sb}}\right)\frac{u_{pb} - u_{sb}}{P_H - P_R} + \left(\frac{\partial P_R}{\partial U_{sb}}\right)\frac{(u_{pb} - u_{ps})^2}{(P_H - P_R)^2}$$

It is assumed throughout the analysis that errors in initial densities of the sample, buffer, and driver and in the assumed equations of state for the latter contribute negligibly to the overall uncertainty in derived parameters.

Acknowledgments. This study would not have been possible without the efforts of T. J. Shankland in providing sample material via an NSF-supported program. We are grateful to H. Richeson, E. Gelle, and R. Smith for their expert technical assistance with all facets of the experimental work and to R. Jeanloz, R. S. Anderssen, J. R. Cleary, L. Liu, R. T. Merrill, and A. E. Ringwood for stimulating discussions of many aspects of this work. The experimental work reported in this paper was performed in the Helen and Roland Lindhurst Laboratory of Experimental Geophysics. This paper was written after one of us (I.J.) took an appointment at the Australian National University. Financial support through the U.S. National Science Foundation (DES 75-15006) is gratefully acknowledged. Contribution number 3048, Division of Geological and Planetary Sciences, California Institute of Technology, Pasadena, California.

REFERENCES

Ahrens, T. J., and C. F. Petersen, Shock wave data and the study of the earth, in *The Application of Modern Physics to the Earth and Planetary Interiors*, edited by S. K. Runcorn, pp. 449–461, John Wiley, New York, 1969.

Ahrens, T. J., D. L. Anderson, and A. E. Ringwood, Equations of state and crystal structures of high-pressure phases of shocked silicates and oxides, *Rev. Geophys., 7*, 667–707, 1969*a*.

Ahrens, T. J., C. F. Petersen, and J. T. Rosenberg, Shock compression of feldspars, *J. Geophys. Res., 74*, 2727–2746, 1969*b*.

Ahrens, T. J., J. H. Lower, and P. L. Lagus, Equation of state of forsterite, *J. Geophys. Res., 76*, 518–528, 1971.

Ahrens, T. J., I. Jackson, and R. Jeanloz, Shock compression and adiabatic release of a titaniferous mare basalt, *Proc. Lunar Sci. Conf. 8th*, 3437–3455, 1977.

Al'tshuler, L. V., and I. I. Sharipdzhanov, Additive equations of state of silicates at high pressures, *Izv. Phys. Solid Earth, 3*, 11–28, 1971.

Anderson, D. L., and H. Kanamori, Shock wave equations of state of rocks and minerals, *J. Geophys. Res., 73*, 6477–6502, 1968.

Anderson, O. L., E. Schreiber, R. C. Leibermann, and N. Soga, Some elastic constant data on minerals relevant to geophysics, *Rev. Geophys., 6*, 491–524, 1968.

Birch, F., The velocity of compressional waves in rocks to 10 kilobars, 1, *J. Geophys. Res., 65*, 1083–1102, 1960.

Birch, F., The velocities of compressional waves in rocks to 10 kilobars, 2, *J. Geophys. Res., 66*, 2199–2224, 1961.

Cleary, J. R., and R. S. Anderssen, Seismology and the internal structure of the earth, in *The Earth: Its Origin, Structure and Evolution*, edited by M. W. McElhinny, Academic, New York, in press, 1979.

Davies, G. F., Quasiharmonic finite-strain equations of state of solids, *J. Phys. Chem. Solids, 34*, 1417–1429, 1973.

Davies, G. F., Limits on the constitution of the lower mantle, *Geophys. J. Roy. Astron. Soc., 38*, 479–504, 1974.

Davies, G. F., and D. L. Anderson, Revised shock wave equations of state for high-pressure phases of rocks and minerals, *J. Geophys. Res., 76*, 2617–2627, 1971.

Davies, G. F., and E. S. Gaffney, Identification of high-pressure phases of rocks and minerals from Hugoniot data, *Geophys. J. Roy. Astron. Soc., 33*, 165–183, 1973.

de Carli, P. S., and J. C. Jamieson, Formation of diamond by explosive shock, *Science, 133*, 1821–1822, 1961.

Dziewonski, A. M., A. L. Hales, and E. R. Lapwood, Parametrically simple earth models consistent with geophysical data, *Phys. Earth Planet. Interiors, 10*, 12–48, 1975.

Grady, D. E., Processes occurring in shock wave compression of rocks and minerals, in *High-Pressure Research: Applications to Geophysics*, edited by M. H. Manghnani and S. Akimoto, Academic, New York, 1977.

Grady, D. E., W. J. Murri, and G. R. Fowles, Quartz to stishovite: Wave propagation in the mixed phase region, *J. Geophys. Res., 79*, 332–338, 1974.

Graham, E. K., and G. R. Barsch, Elastic constants of single-crystal forsterite as a function of temperature and pressure, *J. Geophys. Res., 74*, 5949–5960, 1969.

Hart, R. S., The distribution of seismic velocities and attenuations in the earth, Ph.D. Thesis, Calif. Inst. of Technol., Pasadena, 1977.

Hess, H. H., and A. H. Phillips, Optical properties and chemical composition of magnesian orthopyroxenes, *Amer. Mineral., 25*, 276–285, 1940.

Hill, R., The elastic behaviour of a crystalline aggregate, *Proc. Phys. Soc. London Sect. A, 65*, 349–354, 1952.

Jackson, I., and T. J. Ahrens, The equation of state of forsterite to 160 GPa and its implications for the iron content of the lower mantle (abstract). *Eos Trans. AGU, 58*, 1236, 1977.

Jeanloz, R., and T. J. Ahrens, Pyroxenes and olivines: Structural implications of shock-wave data for high pressure phases, in *High-Pressure Research: Applications to Geophysics*, edited by M. H. Manghnani and S. Akimoto, Academic, New York, 1977*a*.

Jeanloz, R., and T. J. Ahrens, Shocked olivines and the spinel phase, IR spectra, observation and implications (abstract), paper presented at Ninth Annual Meeting, Geol. Soc. of Amer., Seattle, 1977*b*.

Jeanloz, R., T. J. Ahrens, J. S. Lally, G. L. Nord, Jr., J. M. Christie, and A. H. Heuer, Shock-produced olivine glass: First observation, *Science, 147*, 457–459, 1977.

Jenkins, G. M., and D. G. Watts, *Spectral Analysis and Its Applications*, pp. 68–77, Holden-Day, San Francisco, Calif., 1968.

Jones, A. H., W. M. Isbell, and C. J. Maiden, Measurement of the very-high-pressure properties of materials using a light-gas gun, *J. Appl. Phys., 37*, 3493–3499, 1966.

Jones, A. H., W. M. Isbell, F. H. Shipman, R. D. Perkins, S. J. Green, and C. J. Maiden, Material property measurements for selected materials, *Rep. NAS 2-3427*, 56 pp., General Motors Mater. and Struct. Lab., Warren, Mich., 1968.

Kumazawa, M., and O. L. Anderson, Elastic moduli, pressure derivatives, and temperature derivatives of single-crystal olivine and single-crystal forsterite, *J. Geophys. Res., 74*, 5961–5972, 1969.

Liebermann, R. C., A. E. Ringwood, and A. Major, Elasticity of polycrystalline stishovite, *Earth Planet. Sci. Lett., 32*. 127–140, 1976.

Liebermann, R. C., L. E. A. Jones, and A. E. Ringwood, Elasticity of aluminate, titanate, stannate and germanate compounds with the perovskite structure, *Phys. Earth Planet. Interiors, 14*, 165–178, 1977.

Liu, L., Post-oxide phases of forsterite and enstatite, *Geophys. Res. Lett., 2*, 417–419, 1975.

Liu, L., The post-spinel phase of forsterite, *Nature, 262*, 770–772, 1976.

Liu, L., High-pressure $NaAlSiO_4$: The first silicate calcium ferrite isotype, *Geophys. Res. Lett., 4,* 183–186, 1977.

Liu, L., A new high-pressure phase of $Ca_2Al_2SiO_7$ and implications to the earth's interior, *Earth Planet. Sci. Lett., 40,* 401–406, 1978*a*.

Liu, L., A new high-pressure phase of spinel, *Earth Planet. Sci. Lett., 41,* 398–404, 1978*b*.

Lyzenga, G., and T. J. Ahrens, The relation between the shock-induced free surface velocity and the post-shock specific volume of solids, *J. Appl. Phys., 49,* 200–213, 1978.

McQueen, R. G., Shock-wave data and equations of state, in *Seismic Coupling,* edited by G. Simmons, pp. 53–106, Advanced Research Projects Agency Meeting, National Technical Information Service, Springfield, Va., 1968.

McQueen, R. G., and S. P. Marsh, pp. 153–159, in *Handbook of Physical Constants, Geol. Soc. Amer. Mem., 97,* edited by S. P. Clark, Geological Society of America, New York, 1966.

McQueen, R. G., J. N. Fritz, and S. P. Marsh, On the equation of state of stishovite, *J. Geophys. Res., 68,* 2319–2322, 1963.

McQueen, R. G., S. P. Marsh, and J. N. Fritz, Hugoniot equation of state of twelve rocks, *J. Geophys. Res., 72,* 4999–5036, 1967.

McQueen, R. G., S. P. Marsh, J. W. Taylor, J. N. Fritz, and W. J. Carter, The equation of state of solids from shock wave studies, in *High-Velocity Impact Phenomena,* edited by R. Kinslow, pp. 293–417, Academic, New York, 1970.

Ragan, D. M., The twin sisters dunite, Washington, in *Ultramafic and Related Rocks,* edited by P. J. Wyllie, pp. 160–167, John Wiley, New York, 1967.

Rice, M. H., R. G. McQueen, and J. M. Walsh, Compression of solids by strong shock waves, in *Solid State Physics,* vol. 6, edited by F. Seitz and D. Turnbull, pp. 1–63, Academic, New York, 1958.

Ringwood, A. E., *Composition and Petrology of the Earth's Mantle,* p. 188, McGraw-Hill, New York, 1975.

Robie, R. A., P. M. Bethke, M. S. Toulmin, and J. L. Edwards, X-ray crystallographic data, densities, and molar volumes of minerals, in *Handbook of Physical Constants, Geol. Soc. Amer. Mem. 97,* edited by S. P. Clark, Jr., pp. 27–73, Geological Society of America, New York, 1966.

Ross, C. S., M. D. Foster, and A. T. Myers, Origin of dunites and of olivine-rich inclusions in basaltic rocks, *Amer. Mineral., 39,* 693–737, 1954.

Shankland, T. J., Synthetic forsterite, *Bull. Amer. Ceram. Soc., 46,* 1160–1162, 1967.

Spetzler, H., Equation of state of polycrystalline and single-crystal MgO to 8 kilobars and 800°K, *J. Geophys. Res., 75,* 2073–2087, 1970.

Trunin, R. F., V. I. Gon'shakova, G. V. Simakov, and N. E. Galdin, A study of rocks under the high pressures and temperatures created by shock compression, *Izv. Phys. Solid Earth, 9,* 1–12, 1965.

Wackerle, J., Shock-wave compression of quartz, *J. Appl. Phys., 33,* 922–937, 1962.

Wang, C. Y., Constitution of the lower mantle as evidenced from shock wave data for some rocks, *J. Geophys. Res., 73,* 6459–6476, 1968.

Worthington, M. H., The inversion of seismic data using Monte Carlo and linear programming techniques, Ph.D. thesis, 168 pp., Aust. Nat. Univ., Canberra, 1973.

Yagi, T., H. K. Mao, and P. M. Bell, Crystal structure of perovskite-type $MgSiO_3$ (abstract), *Eos Trans. AGU, 58,* 1236, 1977.

Yagi, T., H. K. Mao, and P. M. Bell, Isothermal compression of $MgSiO_3$ perovskite, in Carnegie Institution of Washington Yearbook 77, Carnegie Institution, Washington, D. C., in press, 1978.

(Received June 8, 1978;
revised October 3, 1978;
accepted October 18, 1978.)